Title: Leukocytes have a heparan sulfate glycocalyx that regulates recruitment during inflammation

Authors: Megan J. Priestley,[1] Anna K. Hains,[1] Iashia Z. Mulholland,[1] Sam Spijkers-Shaw,[2, 3] Olga V. Zubkova, [3] Douglas P. Dyer*† [1, 4] & Amy J. Saunders*†[5]

Affiliations:

[1]Wellcome Centre for Cell-Matrix Research, Lydia Becker Institute of Immunology and Inflammation, Faculty of Biology, Medicine and Health, Manchester Academic Health Science Centre, University of Manchester; Manchester, UK.

[2]Department of Chemistry and Chemical Biology, Northeastern University; Boston, MA, United States

[3]The Ferrier Research Institute, Victoria University of Wellington; Gracefield Research Centre, Lower Hutt, New Zealand.

[4]Geoffrey Jefferson Brain Research Centre, Manchester Academic Health Science Centre, Northern Care Alliance NHS Group, University of Manchester; Manchester, United Kingdom.

[5] Division of Biomedical and Life Sciences, Faculty of Medicine and Health, Lancaster University; Lancaster, United Kingdom.

* Corresponding authors. Email: douglas.dyer@manchester.ac.uk, a.saunders@lancaster.ac.uk.

† These authors contributed equally to this work.

Abstract:

The glycocalyx is a proteoglycan-rich layer present on the surface of all mammalian cells that is particularly prevalent on endothelial cells lining the vasculature. It has been hypothesized that the glycocalyx mediates leukocyte migration by masking adhesion molecules and reducing leukocyte adhesion to the endothelium. Leukocyte recruitment is a key driver of inflammatory diseases, including the chronic skin disease, psoriasis. Here, we show that leukocytes express heparan sulfate, an important glycocalyx component, on their cell surface which is lost in response to psoriasis-like skin inflammation, whilst endothelial heparan sulfate expression is not affected. Treatment with a heparan sulfate mimetic during psoriasis-like skin inflammation protected heparan sulfate from cleavage by heparanase and resulted in reduced leukocyte accumulation in skin, yet unexpectedly, led to increased clinical signs of inflammation due to reduced Treg numbers. These findings change our understanding of immune cell recruitment by demonstrating the presence and function of a heparan sulfate glycocalyx on immune cells and urge caution on the use of heparanase inhibitors as therapies for inflammatory diseases.

One Sentence Summary: Leukocytes express a glycocalyx on their surface which is shed in response to psoriasis-like skin inflammation, facilitating their migration into the skin.

Main Text:

INTRODUCTION

During inflammatory disease, excessive recruitment of leukocytes results in aberrant inflammation[1]. The chronic inflammatory skin disease, psoriasis, is associated with the accumulation of large numbers of leukocytes in the dermis, resulting in raised, itchy, and scaly skin lesions[2]. Despite recruitment of immune cells into tissues being a clear driver of inflammation, there are currently no therapeutic strategies targeting leukocyte recruitment as a treatment for psoriasis[3]. In fact, although studied for many years, there are still large gaps in knowledge about the process of leukocyte migration in general[4]. Much research on leukocyte transmigration out of blood vessels has focussed on endothelial cell adhesion molecules such as selectins and immunoglobulin-like adhesion molecules[5], yet much less attention has been paid to the molecules which initiate and regulate the initial interactions between leukocytes and the endothelium; proteoglycans[6].

All mammalian cells likely express proteoglycans on their surface to varying extents, as a part of the cell surface glycocalyx[7]. This layer is formed of core proteins such as syndecans and glypicans, and glycosaminoglycans such as heparan sulfate[8]. Despite glycocalyces being present on the surface of all cells, research until now has focussed heavily on the glycocalyx of the vascular endothelium. Here, the glycocalyx protrudes up to 2 microns from the cell surface[9], making it one of the first layers to come into contact with leukocytes within blood vessels, and potentially regulating early interactions between leukocytes and endothelia[10]. The glycocalyx has also been shown to support chemokine function[11, 12], altering their availability to leukocytes and thereby affecting migration.

However, the glycocalyx is also thought to have anti-adhesive properties due to its shielding of endothelial cell adhesion molecules from binding by leukocytes[9]. During inflammation, the glycocalyx can be shed by factors including shear stress[13], reactive oxygen species[14], and enzymatic degradation by enzymes such as heparanase, which cleaves heparan sulfate from the glycocalyx[15]. This shedding of the endothelial glycocalyx has pro-migratory effects, thought to be due to increased exposure of adhesion molecules which are 'masked' by the glycocalyx at rest[10]. Glycocalyx shedding is associated with several inflammatory conditions including sepsis[16], COVID-19[17], diabetes[18] and recently, psoriasis[19].

Compared to the growing number of studies on the role of the endothelial glycocalyx in inflammatory diseases, very little is known about its counterpart; the leukocyte glycocalyx. Previous studies have shown the presence of proteoglycans, including heparan sulfate proteoglycans, on the surface of leukocytes[20-22], yet little is known about the structure of this layer or its role in the regulation of leukocyte migration.

Here, we show that a model of psoriasis-like skin inflammation is not associated with endothelial HS shedding, however changes were observed in the leukocyte glycocalyx, which was shown to be present on the surface of skin leukocytes *in vivo*. Furthermore, we demonstrate that the use of the heparan sulfate mimetic Tet-29 reduces immune cell recruitment into skin, potentially via its inhibitory action on the heparanase enzyme. Counterintuitively, this reduced immune cell recruitment exacerbated skin inflammation, which may be due to reduced regulatory T cell recruitment. Our findings highlight a novel mechanism for immune cell recruitment *in vivo*, whereby myeloid cells release heparanase and degrade HS on the surface of leukocytes, facilitating their entry into the tissue.

RESULTS

Aldara cream stimulates elevated levels of circulating heparan sulfate but is not associated with endothelial heparan sulfate shedding

During inflammation, leukocytes are recruited into tissues by passing through the vascular endothelium[23]. Therefore, it was hypothesized that the endothelial glycocalyx played a role in psoriasis-like skin inflammation by regulating immune cell recruitment. To assess this, numbers of leukocytes in naïve skin and in psoriasis-like skin inflammation were quantified to determine if immune cells were recruited. Aldara cream was applied topically to the ear pinnae of mice for 6 consecutive days (**Fig 1A**), which led to visible erythema (redness) and scaling of the skin (**Fig 1B**), epidermal thickening **(Fig 1C, D)**, and increased clinical signs of inflammation (**Fig S1A, B, C**) as shown previously[24, 25]. Crucially, Aldara cream induced the accumulation of large numbers of CD45+ cells into skin, peaking at day 6 (**Fig 1E**), with significantly higher numbers of dendritic cells, MHCII+ macrophages, monocytes, neutrophils, and TCRβ+ T cells in Aldara treated skin compared to naive skin (**Fig 1F**), gating shown in **Fig S2**.

Psoriasis is associated with enhanced angiogenesis[26] which may allow increased migration of leukocytes out of blood vessels and into skin[27]. Similarly, Aldara cream treatment resulted in greater skin vascularisation when compared to naïve skin (**Fig S1D, E, F**). To determine whether these vascular changes are accompanied by changes in the endothelial glycocalyx lining the blood vessel, the level of serum HS was measured by ELISA. Aldara cream treated mice had significantly higher concentrations of HS in their serum compared to naïve mice (**Fig 1G**), an indicator of glycocalyx shedding[7,10].

To determine whether the source of elevated circulating HS was the dermal endothelial glycocalyx, skin sections underwent immunofluorescence staining for HS alongside CD31 as a marker for vascular endothelial cells (**Fig 2A, B**), revealing no significant changes in HS mean fluorescence intensity (MFI) across blood vessels following administration of Aldara cream (**Fig 2C**). HS levels were also similar on naïve and inflamed skin endothelial cells (CD45- CD31+) when examined by flow cytometry (**Fig 2D, E**), although the possibility of ultrastructural changes cannot be excluded. These data indicate that although heparan sulfate is elevated in the circulation of mice with psoriasis-like skin inflammation, the source does not appear to be the endothelial glycocalyx.

Leukocytes have a cell surface glycocalyx, from which heparan sulfate is lost in response to psoriasis-like skin inflammation

Previous research has suggested several immune subsets including monocytes[20], neutrophils[21] and macrophages[22], may express heparan sulfate on their surface, yet little is known about the function of the leukocyte glycocalyx during inflammation *in vivo*. To determine if the source of circulating HS in inflammation could be immune cells, flow cytometry was used to reveal a clear population of HS+ CD45+ cells in skin (**Fig 3A**), which is reduced in response to psoriasis-like skin inflammation (**Fig 3B**). Uniform Manifold Approximation and Projection (UMAP) visualisation of leukocytes from naïve skin shows widespread expression of HS on the surface of macrophages, monocytes, dendritic cells, T cells, regulatory T cells, and neutrophils (**Fig 3C, D**). Monocytes and neutrophils had the greatest proportion of HS+ cells, as well as the greatest decrease in HS positivity in response to psoriasis-like skin inflammation (**Fig 3E**). A relatively high proportion of

126 regulatory T cells express HS on their surface, however, this was not significantly downregulated
127 under inflammatory conditions (**Fig 3E**).

128 The only mammalian protein capable of cleaving HS along the polysaccharide chain is the endo-
129 glucuronidase, heparanase[28]. Flow cytometric staining for heparanase stored intracellularly in
130 leukocytes revealed that cells of the myeloid lineage had the highest proportion of heparanase
131 positive cells (**Fig 3F**). In particular, a proportion of monocytes show clear heparanase staining
132 (**Fig 3G**) which was reduced with Aldara cream treatment of the skin (**Fig 3H**), possibly indicating
133 its release from the cell. These data suggest that leukocytes have a glycocalyx on their cell surface,
134 which is shed in response to leukocyte-derived heparanase during skin inflammation.

135

136 **The heparan sulfate mimetic Tet-29 lessens heparan sulfate shedding on leukocytes and**
137 **reduces their accumulation in skin during psoriasis-like inflammation**

138 To determine the importance of heparan sulfate loss from the surface of leukocytes, a heparan
139 sulfate mimetic Tet-29 was injected alongside Aldara cream treatment (**Fig 4A**). Zubkova et al.[29]
140 show that Tet-29 is a potent inhibitor and reduces the cleavage of a heparan sulfate
141 pentasaccharide. Here, flow cytometry revealed that Tet-29 partially protected HS on leukocytes
142 during skin inflammation, resulting in a similar proportion of CD45+ cells staining positively for
143 HS in inflamed Tet-29 treated mice as in naïve mice (**Fig 4B**). Furthermore, Tet-29 treatment
144 resulted in reduced circulating HS in the blood during inflammation compared to PBS treated
145 control mice (**Fig 4C**), indicative of reduced glycocalyx shedding.

146 We hypothesised that protecting leukocytes from HS degradation would reduce their migration
147 into skin and as, a result, would lead to reduced psoriasis-like skin inflammation. However, it was
148 found that clinical readouts of inflammation were significantly enhanced with Tet-29
149 administration alongside Aldara cream treatment when compared to mice injected with phosphate-
150 buffered saline (PBS) as a control (**Fig 4D**). Epidermal thickness, a hallmark of psoriasis severity[30],
151 was measured using haematoxylin and eosin (H&E) staining (**Fig 4E**) and was found to be
152 significantly greater in inflamed Tet-29 treated mice compared to inflamed control mice (**Fig 4F**).
153 To investigate why inflammation was increased rather than reduced by Tet-29, flow cytometry
154 was used to examine the number of leukocytes in the skin. Counterintuitively, it was found that
155 overall numbers of CD45+ cells in inflamed Tet-29 treated skin were decreased compared to
156 inflamed PBS treated skin, but were higher than in uninflamed skin (**Fig 4G**), suggesting that Tet-
157 29 partially blocks the accumulation of immune cells in skin in response to inflammation. MHCII+
158 macrophages and neutrophils, were significantly reduced in number in response to Tet-29
159 treatment (**Fig 4H**). Similar effects were seen in inflamed mice treated with a related HS mimetic[31],
160 which also reduced leukocyte recruitment into skin and enhanced inflammation (**Fig S3**). These
161 data suggest that protection of HS on the immune cell surface during psoriasis-like skin
162 inflammation reduces the ability of leukocytes to transmigrate into skin.

163 To investigate why skin inflammation is exacerbated whilst immune cell numbers are reduced in
164 skin in response to Tet-29, the number of skin regulatory T cells (Tregs) was examined. Tregs are
165 an abundant anti-inflammatory cell type in skin, capable of releasing factors such as interleukin-
166 10 (IL-10) to reduce inflammation[32]. Tregs were significantly reduced in number during skin
167 inflammation in Tet-29 treated mice, relative to control mice (**Fig 4I**), suggesting that the heparan
168 sulfate mimetic may reduce the ability of Tregs to enter skin and carry out immunosuppressive

169 functions. Indeed, by ELISA reduced levels of IL-10 were found in Tet-29 treated compared to
170 PBS treated inflamed skin (**Fig 4J**).

171 To confirm that reduced Treg accumulation leads to enhanced inflammation in Tet-29 treated
172 inflamed mouse skin, mice were treated with Aldara cream alongside injection with anti-CD25 to
173 deplete Tregs (**Fig S4A, S4B**). Depletion of Tregs significantly increased signs of inflammation in
174 skin including ear thickness, redness and scaling (**Fig 4K**), epidermal thickening (**Fig S4C, 4L**),
175 and IL-17 production in the ear draining lymph node (**Fig S4D**).

176 In addition to Treg depletion, Tet-29 treatment reduced myeloid cells including MHCII+
177 macrophages and neutrophils in skin, as mentioned above (**Fig 4H**). To determine the impact of
178 neutrophil depletion, an anti-Ly6G antibody was used to deplete neutrophils in the skin of mice
179 with psoriasis-like skin inflammation (**Fig S5A, B**). However, no significant differences in
180 inflammation were observed (**Fig S5D-H**), suggesting that neutrophils do not affect the clinical
181 signs of psoriasis-like skin inflammation. Therefore, in Tet-29 treatment, reduced skin neutrophils
182 will likely not impact the severity of inflammation.

183 iCCR KO mice, lacking CCRs 1, 2, 3 and 5[33] have reduced numbers of myeloid cells in skin
184 following treatment with Aldara cream, including DCs, monocytes and some macrophages (**Fig**
185 **S6B)**. Despite this, the iCCR KO mice showed no differences in psoriasis-like skin inflammation
186 severity compared to littermate controls (**Fig S6E-I**). These findings demonstrate that the
187 recruitment of myeloid cells to the skin does not affect the severity of psoriasis-like skin
188 inflammation and therefore in Tet-29 treated mice, the reduced myeloid cells are unlikely to affect
189 the severity of inflammation.

190 These data indicate that reduced HS shedding from the leukocyte surface in response to psoriasis-
191 like skin inflammation decreases immune cell accumulation in the skin. This exacerbates skin
192 inflammation due to reduced skin Tregs and the associated reduction in anti-inflammatory
193 cytokines.

194

195 **Loss of cell surface heparan sulfate results in reduced monocyte migration *in vitro***

196 To determine whether the loss of cell surface HS on leukocytes during inflammation promotes
197 migration into inflamed tissues, heparan sulfate was enzymatically degraded on the surface of cells
198 from murine bone marrow using bacterial heparinase, and the ability of these cells to migrate
199 towards CCL7 was investigated (**Fig 5A**). Flow staining confirmed the successful degradation of
200 HS on the surface of bone marrow monocytes treated with heparinase (**Fig 5B-C**), and showed
201 that heparinase treatment promotes the migration of monocytes towards chemokine (**Fig 5D**).
202 These data show that leukocytes have an increased ability to migrate when they have reduced HS
203 on their cell surface, providing a potential explanation for how the heparan sulfate mimetic Tet-29
204 may be responsible for reduced numbers of immune cells in the skin during inflammation. This
205 suggests that the reduction in leukocyte HS under inflammatory conditions may *in vivo* be a
206 mechanism to aid the recruitment of immune cells to the site of inflammation.

207

208 **DISCUSSION**

209 The remodelling of the glycocalyx on the endothelium and its role in facilitating leukocyte
210 recruitment has been increasingly studied over the last 20 years, particularly in the context of

211 inflammatory diseases[34]. Yet, little is known about the function of its counterpart; the leukocyte
212 surface glycocalyx, and how it may be altered during inflammation. In the present study, we have
213 demonstrated the presence of a leukocyte glycocalyx *in vivo* and shown its remodelling in response
214 to skin inflammation, suggesting a novel mechanism for *in vivo* leukocyte recruitment into skin.

215 Whilst the breadth of glycocalyx research has expanded in recent years, it remains primarily
216 focussed on the endothelial glycocalyx. Li et al[19] demonstrate that human patients with psoriasis
217 have lower levels of HS on the dermal vascular endothelium than in healthy patients, yet the
218 leukocyte glycocalyces in these patients were not examined. This common focus on the endothelial
219 glycocalyx has produced assumptions. For example, increased levels of circulating glycocalyx
220 components, such as HS and protein cores, are assumed to be indicative of their shed from the
221 endothelial glycocalyx. Our findings of a glycocalyx on the immune cell surface challenge this
222 assumption.

223 We propose that the loss of HS from the leukocyte surface may contribute to the elevated
224 circulating HS found in inflamed mice in our study. Although, it is likely that other cell types
225 contribute to this, including fibroblasts and keratinocytes, both of which produce HS[35]. These data
226 emphasise the importance of more work on the cell-specific function of HS across a variety of cell
227 types.

228 Much of the current literature on heparanase-mediated degradation of the endothelial glycocalyx
229 has focussed on endothelial cells as the primary source of heparanase. Here it was shown that
230 myeloid cells are another important source of the enzyme, a finding supported by Arokiasamy et
231 al[36] who identify macrophages as a key source of heparanase. This suggests a more widespread
232 expression of heparanase and context dependent effects.

233 Having demonstrated the presence of an HS-containing glycocalyx on immune cells, we next
234 examined its function. Enzymatic degradation of leukocyte HS enhanced the cells' ability to
235 migrate through a transwell. Sabri et al[37] showed a similar finding, with THP1 monocytes shedding
236 a proportion of their cell surface glycocalyx in response to IFNγ treatment, resulting in increased
237 cell adhesion to antibody-coated spheres. Shedding the leukocyte glycocalyx may result in
238 increased exposure of chemokine receptors on the cell surface, allowing monocytes to more readily
239 bind chemokines, resulting in enhanced migration (**Fig 6**). *In vivo*, leukocyte glycocalyx shedding
240 may also expose cell surface adhesion molecules, allowing for greater adhesion to endothelial cells
241 and subsequent transmigration. However, other *in vitro* studies[38, 39] show opposite effects of HS in
242 migration, with reduced glycosaminoglycans on the cell surface associated with their reduced
243 ability to bind chemokine. These data suggest the functions of leukocyte glycocalyx shedding may
244 be context dependent and complex beyond simply shielding and exposing adhesion molecules.

245 Over recent years, heparanase inhibitors have been developed to treat inflammatory diseases[40-42]
246 and cancers[43-46]. Our data supports the idea that the HS mimetic, Tet-29, inhibits heparanase *in*
247 *vivo*. Peck et al.[47] treated mice with Tet-29 during a model of multiple sclerosis which resulted in
248 reduced leukocyte recruitment in the central nervous system. Here, we expand on these findings
249 by providing a potential mechanism for how it may do so, via the protection of HS on the leukocyte
250 surface. However, it is important to note that Tet-29 may also affect other components of the
251 migration process such as binding to cytokines[48], chemokines[11] or integrins[49]. Our findings urge
252 caution on the use of heparanase inhibitors as treatments for inflammatory disease and cancers,
253 due to the enhanced skin inflammation in response to Tet-29 seen here. We hypothesise that in our
254 model, pro-inflammatory cell recruitment is not the sole driver of inflammation, as $\gamma\delta$ T cells and

255 group 3 innate lymphoid cells which drive the inflammation[50] are largely skin resident[51], yet Tregs
256 are more dependent on recruitment to the skin[52]. Therefore, reducing immune cell recruitment to
257 the skin using Tet-29 in this model only marginally affects pro-inflammatory cell activity, but
258 more staunchly affects anti-inflammatory Treg migration, resulting in the enhanced inflammation
259 observed here.

260 Based on our findings, we propose that the recruitment of monocytes into skin during psoriasis-
261 like skin inflammation and their release of heparanase results in the cleavage of HS, allowing
262 subsequent immune cells to migrate into skin more readily (**Fig 6**), a finding supported by previous
263 studies[53-56]. Furthermore, monocytes may be able to cleave HS on their own cell surfaces, as well
264 as on the surface of other immune cells, in order to facilitate their recruitment to inflamed skin.
265 Together, these findings demonstrate the importance of HS proteoglycans in regulating leukocyte
266 recruitment in inflammatory disease. However, they challenge the model that these proteoglycans
267 are primarily endothelial and emphasise the importance of HS on leukocytes themselves.

268

269 MATERIALS AND METHODS

270 *Mice*

271 All animal experiments were locally ethically approved and performed in accordance with the UK
272 Home Office Animals (Scientific Procedures) Act 1986. C57BL/6 mice were obtained from
273 Charles River Laboratories. ICCR KO mice were created by Professor Gerard Graham (University
274 of Glasgow, UK) on a C57BL/6N background[31] and were bred and maintained in specific
275 pathogen-free conditions in house. Mice were 7-14 weeks old and female, except for ICCR mice
276 which were mixed sex.

277 *Induction of psoriasis-like skin inflammation*

278 Psoriasis-like skin inflammation was induced as previously described in Linley et al[24]. Briefly,
279 mice were anaesthetised and treated daily with 10 mg of Aldara cream (Meda Pharmaceuticals)
280 containing 5% Imiquimod, by topical application on both ear pinnae for 6 days (days 0 to 5). Ear
281 thickness was measured daily using a digital micrometer (Mitutoyo) and ear scaling and redness
282 scored daily.

283 *Glycocalyx and Immune cell modulation*

284 *Heparanase inhibition*. To inhibit degradation of heparan sulfate, mice were injected
285 intraperitoneally with 600 µg of the heparan sulfate mimetic Tet-29[28], kindly provided by Dr Olga
286 Zubkova (University of Wellington, New Zealand), or with phosphate buffered saline as a control,
287 daily for 7 days (days -1 to 5).

288 *Regulatory T cell depletion*. Mice were injected intraperitoneally with 250 µg anti-CD25 antibody
289 (BioXCell, clone PC-61.5.3) or with phosphate buffered saline as a control, on days -2, 0, 2 and 4,
290 alongside Aldara cream treatment (given on days 0 to 5, as described above).

291 *Neutrophil depletion*. Mice were injected intraperitoneally with 500 µg anti-Ly6G antibody
292 (BioXCell, clone 1A8) or with 500 µg isotype control (BioXCell), on days -2, 0, 2 and 4, alongside
293 Aldara cream treatment (given on days 0 to 5, as described above).

294 *Haematoxylin and eosin staining*

295 Ear tissue was fixed in 10% neutral buffered formalin (Sigma Aldrich), then embedded in paraffin
296 and cut to 5 µm. Haematoxylin and eosin staining was carried out using an automated Shandon
297 Varistain V24-4. Images were acquired using a 3D HISTECH Pannoramic-250 microscope slide-
298 scanner (3D HISTECH). Snapshots and measurements were taken with Case Viewer software (3D
299 HISTECH). Thickness measurements of both the epidermis and of the whole ear were taken at 3
300 different points on each section, and epidermal thickness was quantified as a percentage of total
301 skin thickness. At least 3 sections were measured per mouse and data points represent the mean
302 epidermal thickness per mouse.

303 ***Cell isolation***

304 Ears were removed from euthanised mice and were split in half. Tissue was digested with 0.5
305 mg/ml DNAse I (Roche) and 0.25 mg/ml Liberase TM (Roche) in complete RPMI (RPMI-1640
306 (Sigma-Aldrich) supplemented with 10% heat-inactivated FBS (Life Technologies Ltd), 1%
307 Penicillin-Streptomycin solution, 1 mM Sodium Pyruvate, 2 mM L-glutamine, 25 nM 2-β-
308 mercaptoethanol, 1x non-essential amino acid solution, 20 mM HEPES buffer; (all Sigma-
309 Aldrich)), shaking for 2 hours at 37ºC before disaggregation in a Medimachine System (BD
310 BioSciences) for 6 minutes. Debris was removed by filtering through a 70 µm cell strainer before
311 cells were washed and counted using Trypan blue exclusion and a haemocytometer.

312 Ear-draining (auricular) lymph nodes (LN) were collected from mice in complete RPMI and single
313 cell suspensions were acquired by gentle agitation on a 70µm strainer.

314 Blood samples were collected via cardiac puncture under terminal anaesthesia and were placed
315 directly into in EDTA (Lonza). Red blood cells were lysed using ammonium-chloride-potassium
316 (ACK) lysis buffer (Lonza).

317 Bone marrow cells were collected by centrifugation of fibulas and tibias, then red blood cells were
318 lysed using ACK lysis buffer (Lonza).

319 ***Flow Cytometric analysis***

320 Cells examined for cytokine production were resuspended in a stimulation media made of
321 complete RPMI (see above) plus 10 µM Brefeldin A, 50 ng/mL phorbol 12-myristate 13-acetate
322 (PMA) and 500 ng/mL ionomycin (all Sigma Aldrich) and incubated for 4 hours at 37 °C. Cells
323 were incubated with a Live/dead blue fixable stain (Invitrogen, ThermoFisher Scientific) diluted
324 to 1:2000 with PBS and Fc block (see **Table S1**) then stained with extracellular antibodies (**Table**
325 **S1**) in FACS wash (PBS with 1% FBS and 2mM EDTA). Cells were fixed using
326 Foxp3/transcription factor staining buffer set (eBioscience). Where indicated, overnight staining
327 using a biotinylated anti-heparan sulfate antibody (**Table S1**) followed by a secondary
328 fluorescently labelled streptavidin antibody (**Table S1**) was performed. Where intracellular
329 staining was performed, cells were permeabilised using the Foxp3/transcription factor staining
330 buffer set (eBioscience) and cells were incubated for 2h in intracellular antibodies (* in **Table S1**)
331 in permeabilisation buffer (eBioscience). Where appropriate, cells were also stained with an anti-
332 rabbit IgG to detect the anti-heparanase antibody (**Table S1**). Data were acquired with a Fortessa
333 X20 (Becton Dickinson) flow cytometer using BD FACSDiva Software. Data were analysed using
334 FlowJo (version 10.8.0) (Treestar Inc.) Gating on cells was carried out according to the gating
335 strategy in **Fig S2**.

336

337 **Uniform manifold approximation and projection (UMAP) clustering**

338 UMAP plots were generated using R[57] by clustering cells based on expression of the markers
339 CD11b, CD11c, CD3, F4/80, Foxp3, Ly6C, Ly6G, MHCII, TCRβ and TCRγδ.

340 ***Enzyme-linked immunosorbent assay (ELISA)***

341 Skin was snap frozen before bead beating using a TissueLyser II (Qiagen) at 20 Hz for 2 minutes
342 with a 5mm ball bearing. Tissue was then placed in lysis buffer (0.1% Triton X100 (Sigma-
343 Aldrich) with cOmplete mini protease inhibitors (Roche) in phosphate buffered saline) for 30
344 minutes at 4 °C.

345 Blood samples were taken from mice by cardiac puncture under terminal anaesthesia and left on
346 ice to coagulate for 4 hours. Blood was centrifuged at 15,000 x g for 10 mins at 4 °C and
347 supernatants collected and frozen.

348 Levels of heparan sulfate and interleukin-10 were measured using enzyme-linked immunosorbent
349 assay kits from Finetest and R&D systems respectively. Data depicts the mean of duplicates for
350 each sample.

351 **Immunofluorescence staining**

352 Sections were dewaxed in xylene and rehydrated in decreasing concentrations of ethanol. Antigen
353 retrieval was carried using Tris-EDTA buffer (pH 9.0) before permeabilization in 0.5 % Triton-
354 X100 (Sigma-Aldrich). Sections were blocked using donkey serum in 1% BSA for 30 mins at
355 room temperature, then using an Avidin/Biotin blocking kit (Vector) according to manufacturer's
356 instructions. Sections were further blocked using Mouse Ig Blocking Reagent (Mouse on Mouse
357 Immunodetection Kit, Vector) for 1 hour. Sections were incubated with primary antibodies (**Table**
358 **S2**) overnight at 4 degrees, followed by anti-heparan sulfate antibody (**Table S2**) for 10 minutes,
359 followed by tertiary antibodies against HS and secondary antibodies against CD31 (**Table S2**) for
360 1 hour at room temperature, all made up in MOM diluent (Mouse on Mouse Immunodetection Kit,
361 Vector). Nuclei were visualised using DAPI (49,6-diamidino-2-phenylindole) (Thermofisher)
362 staining (0.2 µg/ml for 5 minutes) and sections were mounted using Prolong Gold antifade
363 mountant (Thermofisher). Images were collected on a Zeiss Axioimager.D2 upright microscope
364 using 10x, 20x, 40x and 63x EC Plan-neofluar objective lenses and captured using a Coolsnap
365 HQ2 camera (Photometrics) through Micromanager software v1.4.23. Images were processed and
366 analysed using ImageJ (version 1.53a).

367 **Immunofluorescence image analysis**

368 HS expression was quantified in images by selecting endothelial cells (using CD31) on the
369 perimeter of blood vessels excluding the lumen, and measuring the mean fluorescence value for
370 HS staining within these areas. At least 3 vessels were measured per section and at least 3 sections
371 were measured per mouse. Data represent the MFI (mean fluorescence intensity) per mouse.
372 Vascularisation of skin was quantified by measuring the number of pixels staining positively for
373 CD31 and dividing this by the number of pixels within the boundary of the skin section. At least
374 5 sections were measured per mouse.

375 ***In vitro* heparinase treatment**

376 Bone marrow cells were collected by centrifugation of fibulas and tibias, then red blood cells were
377 lysed using ammonium-chloride-potassium (ACK) lysis buffer (Gibco). Cells were resuspended
378 at 2.5 million cells/mL and treated with 1 U/mL heparinase I and III from flavobacterium
379 heparinum (Sigma-Aldrich) for 6 hours at 37°C in complete RPMI.

380 **Migration experiments**

381 Migration assays were performed using 24-well transwell plates with 5 μm pore size filter inserts
382 (Corning). CCL7 was added to 100 nM in the bottom well in complete RPMI. 100μL bone marrow
383 containing $1.25x10^7$ cells was added to the upper chamber and cells were allowed to migrate for 2
384 hours at 37 °C, before migrated cells were collected and analysed by flow cytometry. The
385 proportion of cells migrated was calculated by dividing the number of migrated cells by the number
386 of cells recovered from a well with no transwell insert. Data are from 2 independent experiments,
387 performed in triplicate.

388 **Statistical Analysis**

389 All data were analysed using GraphPad Prism 10. Data were tested for normality using a Shapiro-
390 Wilks test. Unpaired t tests (2 groups) or one-way ANOVAs with Tukey's multiple comparison
391 test (more than 2 groups) were used for parametric data. Non-parametric data were analysed using
392 Mann-Whitney U tests (2 groups) or Kruskal Wallis with Dunn's multiple comparisons test (more
393 than 2 groups). Data annotated as 'fold change' is normalised as a percentage of the average value
394 of the PBS control group in each experiment.

395

396 **Supplementary Materials**

397 **Figure S1.** *Characterising changes in clinical signs of inflammation and the vasculature during*
398 *psoriasis-like skin inflammation.*

399 **Figure S2**. *Flow cytometry gating strategy for leukocytes and endothelial cells*.

400 **Figure S3.** *A related heparan sulfate mimetic inhibits leukocyte recruitment in skin but enhances*
401 *clinical signs of inflammation.*

402 **Figure S4.** *Anti-CD25 treatment depletes regulatory T cells and enhances some signs of*
403 *inflammation during psoriasis-like skin inflammation.*

404 **Figure S5**. *Depletion of neutrophils does not recapitulate the enhanced inflammation seen with*
405 *heparanase inhibition during psoriasis-like skin inflammation.*

406 **Figure S6**. *Depletion of myeloid cells does not recapitulate the enhanced inflammation seen with*
407 *heparanase inhibition during psoriasis-like skin inflammation.*

408 **Table S1**. *Antibodies used for flow cytometry staining.*

409 **Table S2**. *Antibodies for immunofluorescence staining.*

410

411 **References and Notes**

412 1. NOURSHARGH, S. & ALON, R. 2014. Leukocyte migration into inflamed
413 tissues. Immunity, 41, 694-707.

414 2. HAWKES, J. E., CHAN, T. C. & KRUEGER, J. G. 2017. Psoriasis pathogenesis and the
415 development of novel targeted immune therapies. J Allergy Clin Immunol, 140, 645-653.

3. LANDECK, L., SABAT, R., GHORESCHI, K., MAN, X. Y., FUHRMEISTER, K., GONZALEZ-MARTINEZ, E. & ASADULLAH, K. 2021. Immunotherapy in psoriasis. Immunotherapy, 13, 605-619.

4. KRÜGER-GENGE, A., BLOCKI, A., FRANKE, R. P. & JUNG, F. 2019. Vascular Endothelial Cell Biology: An Update. Int J Mol Sci, 20.

5. SCHIMMEL, L., HEEMSKERK, N. & VAN BUUL, J. D. 2017. Leukocyte transendothelial migration: A local affair. Small GTPases, 8, 1-15.

6. GRAY, A. L., PUN, N., RIDLEY, A. J. L. & DYER, D. P. 2022. Role of extracellular matrix proteoglycans in immune cell recruitment. Int J Exp Pathol, 103, 34-43.

7. SUTHERLAND, T. E., DYER, D. P. & ALLEN, J. E. 2023. The extracellular matrix and the immune system: A mutually dependent relationship. Science, 379, eabp8964.

8. IOZZO, R. V. & SCHAEFER, L. 2015. Proteoglycan form and function: A comprehensive nomenclature of proteoglycans. Matrix Biol, 42, 11-55.

9. REITSMA, S., SLAAF, D. W., VINK, H., VAN ZANDVOORT, M. A. & OUDE EGBRINK, M. G. 2007. The endothelial glycocalyx: composition, functions, and visualization. Pflugers Arch, 454, 345-59.

10. MARKI, A., ESKO, J. D., PRIES, A. R. & LEY, K. 2015. Role of the endothelial surface layer in neutrophil recruitment. J Leukoc Biol, 98, 503-15.

11. GRAY, A. L., KARLSSON, R., ROBERTS, A. R. E., RIDLEY, A. J. L., PUN, N., KHAN, B., LAWLESS, C., LUÍS, R., SZPAKOWSKA, M., CHEVIGNÉ, A., HUGHES, C. E., MEDINA-RUIZ, L., BIRCHENOUGH, H. L., MULHOLLAND, I. Z., SALANGA, C. L., YATES, E. A., TURNBULL, J. E., HANDEL, T. M., GRAHAM, G. J., JOWITT, T. A., SCHIESSL, I., RICHTER, R. P., MILLER, R. L. & DYER, D. P. 2023. Chemokine CXCL4 interactions with extracellular matrix proteoglycans mediate widespread immune cell recruitment independent of chemokine receptors. Cell Rep, 42, 111930.

12. RIDLEY, A. J. L., OU, Y., KARLSSON, R., PUN, N., BIRCHENOUGH, H. L., MULHOLLAND, I. Z., BIRCH, M. L., MACDONALD, A. S., JOWITT, T. A., LAWLESS, C., MILLER, R. L. & DYER, D. P. 2023. Chemokines form complex signals during inflammation and disease that can be decoded by extracellular matrix proteoglycans. Sci Signal, 16, eadf2537.

13. LUPU, F., KINASEWITZ, G. & DORMER, K. 2020. The role of endothelial shear stress on haemodynamics, inflammation, coagulation and glycocalyx during sepsis. J Cell Mol Med, 24, 12258-12271.

14. SINGH, A., RAMNATH, R. D., FOSTER, R. R., WYLIE, E. C., FRIDÉN, V., DASGUPTA, I., HARALDSSON, B., WELSH, G. I., MATHIESON, P. W. & SATCHELL, S. C. 2013. Reactive

450 oxygen species modulate the barrier function of the human glomerular endothelial
451 glycocalyx. PLoS One, 8, e55852.

452 15. MASOLA, V., GRECO, N., GAMBARO, G., FRANCHI, M. & ONISTO, M. 2022.
453 Heparanase as active player in endothelial glycocalyx remodeling. Matrix Biol Plus, 13, 100097.

454 16. SCHMIDT, E. P., YANG, Y., JANSSEN, W. J., GANDJEVA, A., PEREZ, M. J., BARTHEL,
455 L., ZEMANS, R. L., BOWMAN, J. C., KOYANAGI, D. E., YUNT, Z. X., SMITH, L. P.,
456 CHENG, S. S., OVERDIER, K. H., THOMPSON, K. R., GERACI, M. W., DOUGLAS, I. S.,
457 PEARSE, D. B. & TUDER, R. M. 2012. The pulmonary endothelial glycocalyx regulates
458 neutrophil adhesion and lung injury during experimental sepsis. Nat Med, 18, 1217-23.

459 17. YAMAOKA-TOJO, M. 2020. Vascular Endothelial Glycocalyx Damage in COVID-19. Int J
460 Mol Sci, 21.

461 18. PERRIN, R. M., HARPER, S. J. & BATES, D. O. 2007. A role for the endothelial glycocalyx
462 in regulating microvascular permeability in diabetes mellitus. Cell Biochem Biophys, 49, 65-72.

463 19. LI, Q., SHAO, S., ZHU, Z., CHEN, J., HAO, J., BAI, Y., LI, B., DANG, E. & WANG, G.
464 2023. An IGFBP7hi endothelial cell subset drives T cell extravasation in psoriasis via endothelial
465 glycocalyx degradation. J Clin Invest, 133.

466 20. DEN DEKKER, E., GREFTE, S., HUIJS, T., TEN DAM, G. B., VERSTEEG, E. M., VAN
467 DEN BERK, L. C., BLADERGROEN, B. A., VAN KUPPEVELT, T. H., FIGDOR, C. G. &
468 TORENSMA, R. 2008. Monocyte cell surface glycosaminoglycans positively modulate IL-4-
469 induced differentiation toward dendritic cells. J Immunol, 180, 3680-8.

470 21 CAMPBELL, E. J. & OWEN, C. A. 2007. The sulfate groups of chondroitin sulfate- and
471 heparan sulfate-containing proteoglycans in neutrophil plasma membranes are novel binding sites
472 for human leukocyte elastase and cathepsin G. J Biol Chem, 282, 14645-54.

473 22 EBSTEIN, S. Y., RAFIQUE, A., ZHOU, Y., KRASCO, A., MONTALVO-ORTIZ, W., YU,
474 L., CUSTODIO, L., ADAM, R. C., BLOCH, N., LEE, K., ADEWALE, F., VERGATA, D., LUZ,
475 A., COQUERY, S., DANIEL, B., ULLMAN, E., FRANKLIN, M. C., HERMANN, A., HUANG,
476 T., OLSON, W., DAVIS, S., MURPHY, A. J., SLEEMAN, M. A., WEI, J. & SKOKOS, D. 2023.
477 VSIG4 interaction with heparan sulfates inhibits VSIG4-complement
478 binding. Glycobiology, 33, 591-604.

479 23. SUN, H., HU, L. & FAN, Z. 2021. β2 integrin activation and signal transduction
480 in leukocyte recruitment. *Am J Physiol Cell Physiol,* 321, C308-c316.

481 24. VAN DER FITS, L., MOURITS, S., VOERMAN, J. S., KANT, M., BOON, L., LAMAN, J.
482 D., CORNELISSEN, F., MUS, A. M., FLORENCIA, E., PRENS, E. P. & LUBBERTS, E. 2009.
483 Imiquimod-induced psoriasis-like skin inflammation in mice is mediated via the IL-23/IL-17
484 axis. J Immunol, 182, 5836-45.

485 25. LINLEY, H., OGDEN, A., JAIGIRDAR, S., BUCKINGHAM, L., COX, J., PRIESTLEY, M.
486 & SAUNDERS, A. 2023. CD200R1 promotes interleukin-17 production by group 3 innate
487 lymphoid cells by enhancing signal transducer and activator of transcription 3 activation. Mucosal
488 Immunol, 16, 167-179.

489 26. HAN, D., LI, F., ZHAO, Y., WANG, B., WANG, J., LIU, B., MOU, K., MENG, L., ZHENG,
490 Y., LU, S., ZHU, W. & ZHOU, Y. 2024. IL-21 promoting angiogenesis contributes to the
491 development of psoriasis. Faseb j, 38, e23375.

492 27. HEIDENREICH, R., RÖCKEN, M. & GHORESCHI, K. 2009. Angiogenesis drives psoriasis
493 pathogenesis. Int J Exp Pathol, 90, 232-48.

494 28. VLODAVSKY, I., ILAN, N. & SANDERSON, R. D. 2020. Forty Years of Basic and
495 Translational Heparanase Research. Adv Exp Med Biol, 1221, 3-59.

496 29. ZUBKOVA, O. V., AHMED, Y. A., GUIMOND, S. E., NOBLE, S. L., MILLER, J. H.,
497 ALFRED SMITH, R. A., NURCOMBE, V., TYLER, P. C., WEISSMANN, M., VLODAVSKY,
498 I. & TURNBULL, J. E. 2018. Dendrimer Heparan Sulfate Glycomimetics: Potent Heparanase
499 Inhibitors for Anticancer Therapy. *ACS Chem Biol,* 13**,** 3236-3242.

500 30. GANGWAR, R. S., GUDJONSSON, J. E. & WARD, N. L. 2022. Mouse Models of Psoriasis:
501 A Comprehensive Review. J Invest Dermatol, 142, 884-897.

502 31. SPIJKERS-SHAW, S., CAMPBELL, K., SHIELDS, N. J., MILLER, J. H., RENDLE, P. M.,
503 JIAO, W., YOUNG, S. L. & ZUBKOVA, O. V. 2022. Synthesis of Novel Glycolipid Mimetics of
504 Heparan Sulfate and Their Application in Colorectal Cancer Treatment in a Mouse Model. Chem
505 Asian J, 17, e202200228.

506 32. RUBTSOV, Y. P., RASMUSSEN, J. P., CHI, E. Y., FONTENOT, J., CASTELLI, L., YE, X.,
507 TREUTING, P., SIEWE, L., ROERS, A., HENDERSON, W. R., JR., MULLER, W. &
508 RUDENSKY, A. Y. 2008. Regulatory T cell-derived interleukin-10 limits inflammation at
509 environmental interfaces. Immunity, 28, 546-58.

510 33. DYER, D. P., MEDINA-RUIZ, L., BARTOLINI, R., SCHUETTE, F., HUGHES, C. E.,
511 PALLAS, K., VIDLER, F., MACLEOD, M. K. L., KELLY, C. J., LEE, K. M., HANSELL, C. A.
512 H. & GRAHAM, G. J. 2019. Chemokine Receptor Redundancy and Specificity Are Context
513 Dependent. Immunity, 50, 378-389.e5.

514 34. KOLÁŘOVÁ, H., AMBRŮZOVÁ, B., SVIHÁLKOVÁ ŠINDLEROVÁ, L., KLINKE, A. &
515 KUBALA, L. 2014. Modulation of endothelial glycocalyx structure under inflammatory
516 conditions. *Mediators Inflamm,* 2014**,** 694312.

517 35. SMITH, M. M. & MELROSE, J. 2015. Proteoglycans in Normal and Healing Skin. Adv
518 Wound Care (New Rochelle), 4, 152-173.

519 36. AROKIASAMY, S., KING, R., BOULAGHRASSE, H., POSTON, R. N., NOURSHARGH,
520 S., WANG, W. & VOISIN, M. B. 2019. Heparanase-Dependent Remodeling of Initial Lymphatic
521 Glycocalyx Regulates Tissue-Fluid Drainage During Acute Inflammation in vivo. Front
522 Immunol, 10, 2316.

523 37. SABRI, S., SOLER, M., FOA, C., PIERRES, A., BENOLIEL, A. & BONGRAND, P. 2000.
524 Glycocalyx modulation is a physiological means of regulating cell adhesion. J Cell Sci, 113 (Pt
525 9), 1589-600.

526 38. GOLDBLATT, J., LAWRENSON, R. A., MUIR, L., DATTANI, S., HOFFLAND, A.,
527 TSUCHIYA, T., KANEGASAKI, S., SRISKANDAN, S. & PEASE, J. E. 2019. A Requirement
528 for Neutrophil Glycosaminoglycans in Chemokine:Receptor Interactions Is Revealed by the
529 Streptococcal Protease SpyCEP. J Immunol, 202, 3246-3255.

530 39. SALANGA, C. L., DYER, D. P., KISELAR, J. G., GUPTA, S., CHANCE, M. R. & HANDEL,
531 T. M. 2014. Multiple glycosaminoglycan-binding epitopes of monocyte chemoattractant protein-
532 3/CCL7 enable it to function as a non-oligomerizing chemokine. J Biol Chem, 289, 14896-912.

533 40. ABASSI, Z., HAMOUD, S., HASSAN, A., KHAMAYSI, I., NATIV, O., HEYMAN, S. N.,
534 MUHAMMAD, R. S., ILAN, N., SINGH, P., HAMMOND, E., ZAZA, G., LUPO, A., ONISTO,
535 M., BELLIN, G., MASOLA, V., VLODAVSKY, I. & GAMBARO, G. 2017. Involvement of
536 heparanase in the pathogenesis of acute kidney injury: nephroprotective effect of
537 PG545. *Oncotarget,* 8**,** 34191-34204.

538 41. CHEN, S., HE, Y., HU, Z., LU, S., YIN, X., MA, X., LV, C. & JIN, G. 2017. Heparanase
539 Mediates Intestinal Inflammation and Injury in a Mouse Model of Sepsis. *J Histochem*
540 *Cytochem,* 65**,** 241-249.

541 42. GAMEZ, M., ELHEGNI, H. E., FAWAZ, S., HO, K. H., CAMPBELL, N. W., COPLAND,
542 D. A., ONIONS, K. L., BUTLER, M. J., WASSON, E. J., CROMPTON, M., RAMNATH, R. D.,
543 QIU, Y., YAMAGUCHI, Y., ARKILL, K. P., BATES, D. O., TURNBULL, J. E., ZUBKOVA,
544 O. V., WELSH, G. I., ATAN, D., SATCHELL, S. C. & FOSTER, R. R. 2024. Heparanase
545 inhibition as a systemic approach to protect the endothelial glycocalyx and prevent microvascular
546 complications in diabetes. *Cardiovasc Diabetol,* 23**,** 50.

547 43. BARASH, U., RANGAPPA, S., MOHAN, C. D., VISHWANATH, D., BOYANGO, I.,
548 BASAPPA, B., VLODAVSKY, I. & RANGAPPA, K. S. 2021. New Heparanase-Inhibiting
549 Triazolo-Thiadiazoles Attenuate Primary Tumor Growth and Metastasis. *Cancers (Basel),* 13.

550 44. DE BOER, C., ARMSTRONG, Z., LIT, V. A. J., BARASH, U., RUIJGROK, G., BOYANGO,
551 I., WEITZENBERG, M. M., SCHRODER, S. P., SARRIS, A. J. C., MEEUWENOORD, N. J.,
552 BULE, P., KAYAL, Y., ILAN, N., CODEE, J. D. C., VLODAVSKY, I., OVERKLEEFT, H. S.,
553 DAVIES, G. J. & WU, L. 2022. Mechanism-based heparanase inhibitors reduce cancer metastasis
554 in vivo. *Proc Natl Acad Sci U S A,* 119**,** e2203167119.

555 45. SINGH, P., BLATT, A., FELD, S., ZOHAR, Y., SAADI, E., BARKI-HARRINGTON, L.,
556 HAMMOND, E., ILAN, N., VLODAVSKY, I., CHOWERS, Y. & HALF, E. 2017. The
557 Heparanase Inhibitor PG545 Attenuates Colon Cancer Initiation and Growth, Associating with
558 Increased p21 Expression. *Neoplasia,* 19**,** 175-184.

559 46. WEISSMANN, M., ARVATZ, G., HOROWITZ, N., FELD, S., NARODITSKY, I., ZHANG,
560 Y., NG, M., HAMMOND, E., NEVO, E., VLODAVSKY, I. & ILAN, N. 2016. Heparanase-
561 neutralizing antibodies attenuate lymphoma tumor growth and metastasis. *Proc Natl Acad Sci U S*
562 *A,* 113**,** 704-9.

563 47. PECK, T., DAVIS, C., LENIHAN-GEELS, G., GRIFFITHS, M., SPIJKERS-SHAW, S.,
564 ZUBKOVA, O. V. & LA FLAMME, A. C. 2023. The novel HS-mimetic, Tet-29, regulates
565 immune cell trafficking across barriers of the CNS during inflammation. *J*
566 *Neuroinflammation,* 20**,** 251.

567 48. XIE, M. & LI, J. P. 2019. Heparan sulfate proteoglycan - A common receptor for
568 diverse cytokines. *Cell Signal,* 54**,** 115-121.

569 49. HASSAN, N., GREVE, B., ESPINOZA-SÁNCHEZ, N. A. & GÖTTE, M. 2021.
570 Cell-surface heparan sulfate proteoglycans as multifunctional integrators of
571 signaling in cancer. *Cell Signal,* 77**,** 109822.

572 50. PANTELYUSHIN, S., HAAK, S., INGOLD, B., KULIG, P., HEPPNER, F. L., NAVARINI,
573 A. A. & BECHER, B. 2012. Rorγt+ innate lymphocytes and γδ T cells initiate psoriasiform plaque
574 formation in mice. J Clin Invest, 122, 2252-6.

575 51. DUTTON, E. E., GAJDASIK, D. W., WILLIS, C., FIANCETTE, R., BISHOP, E. L.,
576 CAMELO, A., SLEEMAN, M. A., COCCIA, M., DIDIERLAURENT, A. M., TOMURA, M.,
577 PILATAXI, F., MOREHOUSE, C. A., CARLESSO, G. & WITHERS, D. R. 2019. Peripheral
578 lymph nodes contain migratory and resident innate lymphoid cell populations. Sci Immunol, 4.

579 52. NORMAN, M. U., CHOW, Z., SNELGROVE, S. L., PRAKONGTHAM, P. & HICKEY, M.
580 J. 2021. Dynamic Regulation of the Molecular Mechanisms of Regulatory T Cell Migration in
581 Inflamed Skin. Front Immunol, 12, 655499.

582 53. POON, I. K., GOODALL, K. J., PHIPPS, S., CHOW, J. D., PAGLER, E. B., ANDREWS, D.
583 M., CONLAN, C. L., RYAN, G. F., WHITE, J. A., WONG, M. K., HORAN, C., MATTHAEI, K.
584 I., SMYTH, M. J. & HULETT, M. D. 2014. Mice deficient in heparanase exhibit impaired
585 dendritic cell migration and reduced airway inflammation. Eur J Immunol, 44, 1016-30.

586 54. PUTZ, E. M., MAYFOSH, A. J., KOS, K., BARKAUSKAS, D. S., NAKAMURA, K.,
587 TOWN, L., GOODALL, K. J., YEE, D. Y., POON, I. K., BASCHUK, N., SOUZA-FONSECA-
588 GUIMARAES, F., HULETT, M. D. & SMYTH, M. J. 2017. NK cell heparanase controls tumor
589 invasion and immune surveillance. J Clin Invest, 127, 2777-2788

590 55. SASAKI, N., HIGASHI, N., TAKA, T., NAKAJIMA, M. & IRIMURA, T. 2004. Cell surface
591 localization of heparanase on macrophages regulates degradation of extracellular matrix heparan
592 sulfate. J Immunol, 172, 3830-5.

593 56. MAYFOSH, A. J., GOODALL, K. J., NGUYEN, T., BASCHUK, N. & HULETT, M. D. 2022.
594 Heparanase is a regulator of natural killer cell activation and cytotoxicity. J Leukoc
595 Biol, 111, 1211-1224.

596 57. MCINNES, L., HEALY, J., MELVILLE, J. 2018. UMAP: Uniform Manifold Approximation
597 and Projection for Dimension Reduction. arXiv:1802.03426.

598

599 **Acknowledgments:**

600 The authors acknowledge members of the Saunders lab and Dyer lab for critical discussion. We
601 acknowledge members of the biological services, flow cytometry, histology and bioimaging
602 facilities at the University of Manchester. We acknowledge the gift of ICCR KO mice from
603 Professor Graham from the University of Glasgow. OZ thanks Dr. Andrew Lewis and Dr. Yinrong
604 Lu for an exceptional NMR and mass spectroscopy service, and Ye Li for assistance with the
605 synthesis. Diagrams created using Biorender.com.

606 **Funding:**

607 Sir Henry Dale fellowship jointly funded by the Wellcome Trust and Royal Society 218570/Z/19/Z
608 (DD)

609 Wellcome Trust center grant 203128/A/16/Z (DD)

610 Sir Henry Dale fellowship jointly funded by the Wellcome Trust and Royal Society 109375/Z/15/Z
611 (AS)

612 New Zealand Ministry of Business, Innovation and Employment RTVU1801 (OZ)

613 New Zealand Breast Cancer Foundation R1703 (OZ)

614 Wellcome Trust Immunomatrix in Complex Disease (ICD) PhD studentship 218491/Z/19/Z (MP)

615 **Author contributions:**

616 Conceptualization: MP, DD, AS

617 Methodology: MP, IM, AS, DD

618 Investigation: MP, AH, AS, DD

619 Visualization: MP

620 Resources: OZ, SSS

621 Funding acquisition: DD, AS

622 Project administration: DD, AS

623 Supervision: DD, AS

624 Writing – original draft: MP

Writing – review & editing: MP, DD, AS, SSS

Competing interests: Authors declare that they have no competing interests.

Data and materials availability: Any data not explicitly evident in the paper will be available on reasonable request.

Figures:

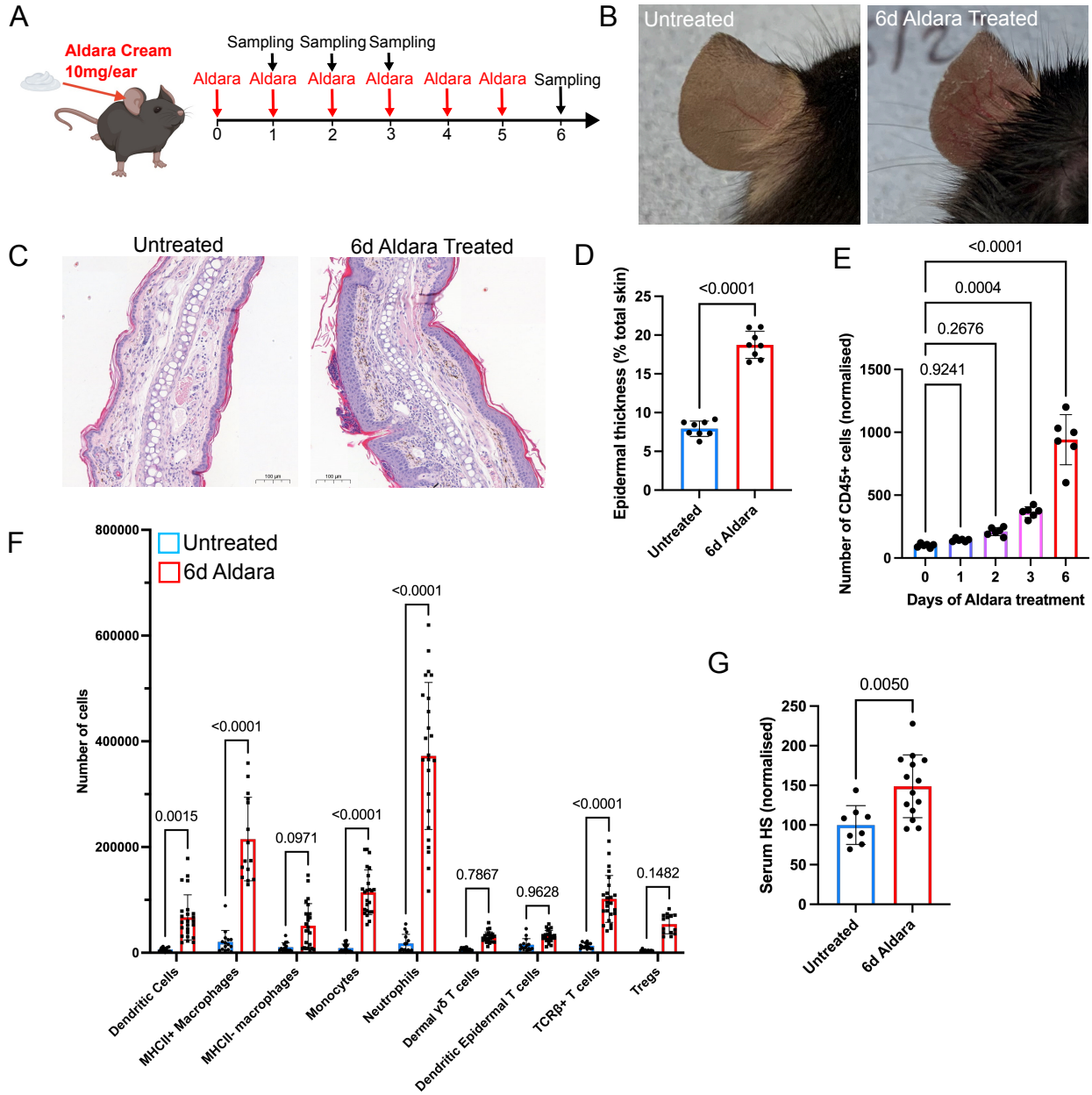

Figure 1. *Topical application of Aldara cream stimulates immune cell accumulation in skin and elevates serum heparan sulfate.* Mice were treated with topical application of 10 mg Aldara cream to each ear pinnae daily for 0-6 days (**A**) to induce skin inflammation (**B**). Skin was sectioned and

635 stained using haematoxylin and eosin (H&E) (**C**) and epidermal thickness measured from these
636 images and calculated as a % of total ear thickness (**D**). The number of CD45+ cells normalised to
637 the mean of untreated controls (**E**) and numbers of dendritic cells, macrophages, monocytes,
638 neutrophils and T cells (**F**) were quantified on day 6 of Aldara treatment in both ears by flow
639 cytometry. Circulating HS in the blood was measured by ELISA and normalised to the untreated
640 control (**G**). Histology scale bars represent 100 μm. Data are pooled from 3 independent
641 experiments, except for **F** which is pooled from 4 independent experiments. Each point represents
642 individual mouse data. **B and C** show representative images from one experiment, with **C** at 10x
643 magnification. Data in **D and G** were analysed by unpaired t test, **E** by one-way ANOVA with
644 Tukey's multiple comparisons test and **F** by 2-way ANOVA with Tukey's multiple comparisons
645 test. Error bars represent mean ± SD.

646

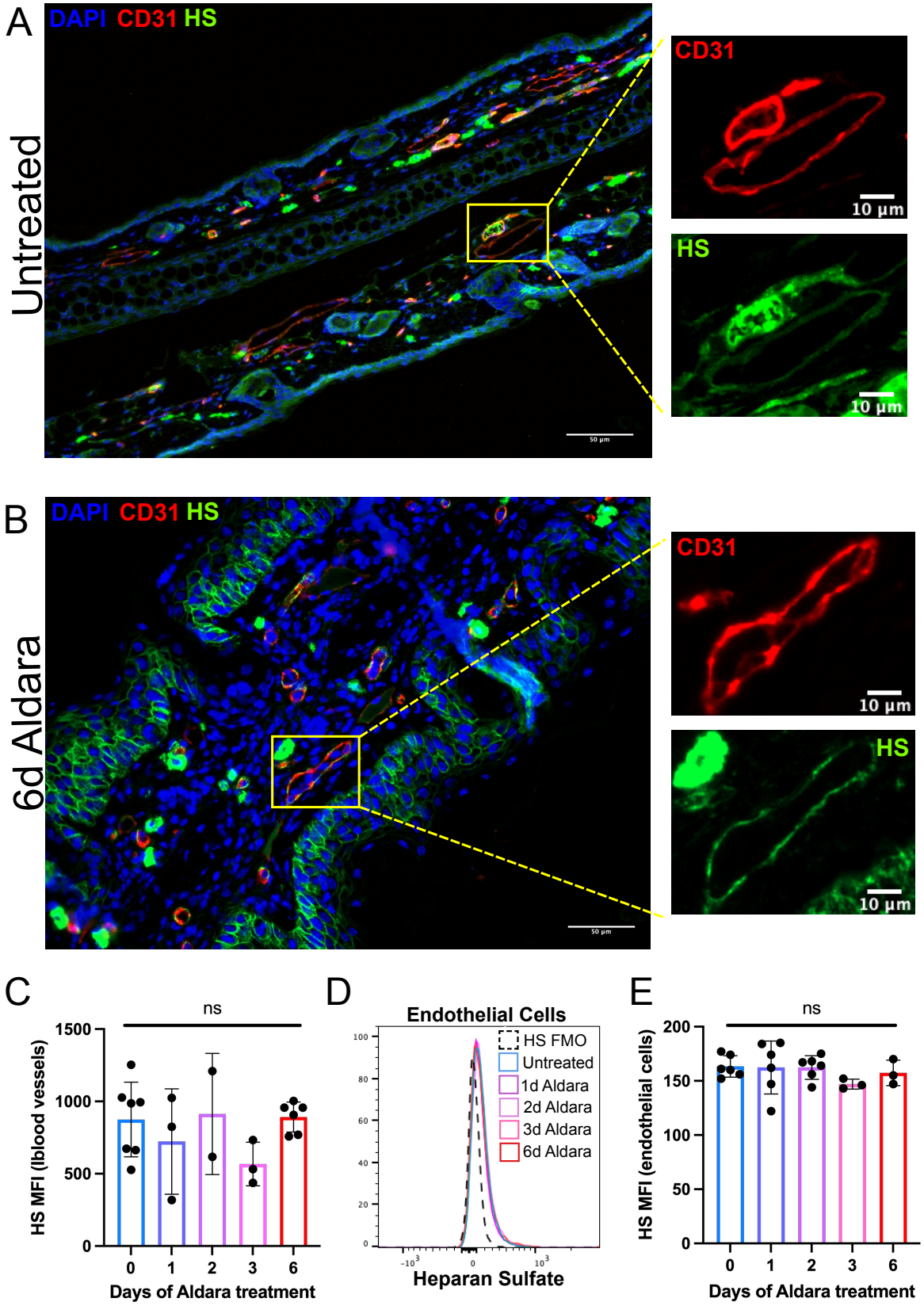
A
DAPI CD31 HS
Untreated
CD31
10 µm
HS
10 µm
B
DAPI CD31 HS
6d Aldara
CD31
10 µm
HS
10 µm
C
ns
HS MFI (lblood vessels)
1500
1000
500
0
0 1 2 3 6
Days of Aldara treatment
D
Endothelial Cells
HS FMO
Untreated
1d Aldara
2d Aldara
3d Aldara
6d Aldara
Heparan Sulfate
E
ns
HS MFI (endothelial cells)
200
150
100
50
0
0 1 2 3 6
Days of Aldara treatment

647

648 **Figure 2.** *Heparan sulfate in the endothelial glycocalyx is unchanged in response to psoriasis-like*
649 *skin inflammation.* Mice were treated with daily topical application of Aldara cream for 0, 1, 2, 3
650 or 6 days on both ear pinnae. Skin was stained for HS (green), CD31 (red) and DAPI (blue) (**A,**
651 **B**) and mean MFI of HS staining measured within the vessel using imageJ (**C**). HS expression on
652 endothelial cells (CD45- CD31+) was measured using flow cytometry (**D**) by calculating the
653 geometric mean fluorescence intensity (gMFI) of HS on CD45- CD31+ cells (**E**). Scale bars in the
654 large images in A and B represent 50 μm, and in the small images 10 μm. **C** and **E** show pooled
655 data from 2 experiments. **A and B** are representative images of skin sections, with zoomed in
656 images of individual vessels highlighted by yellow squares. **D** is a histogram representative of 2
657 experiments. Data were analysed by one-way ANOVA with Tukey's multiple comparison test.
658 'ns' denotes not significant. Error bars represent mean ± SD.

659

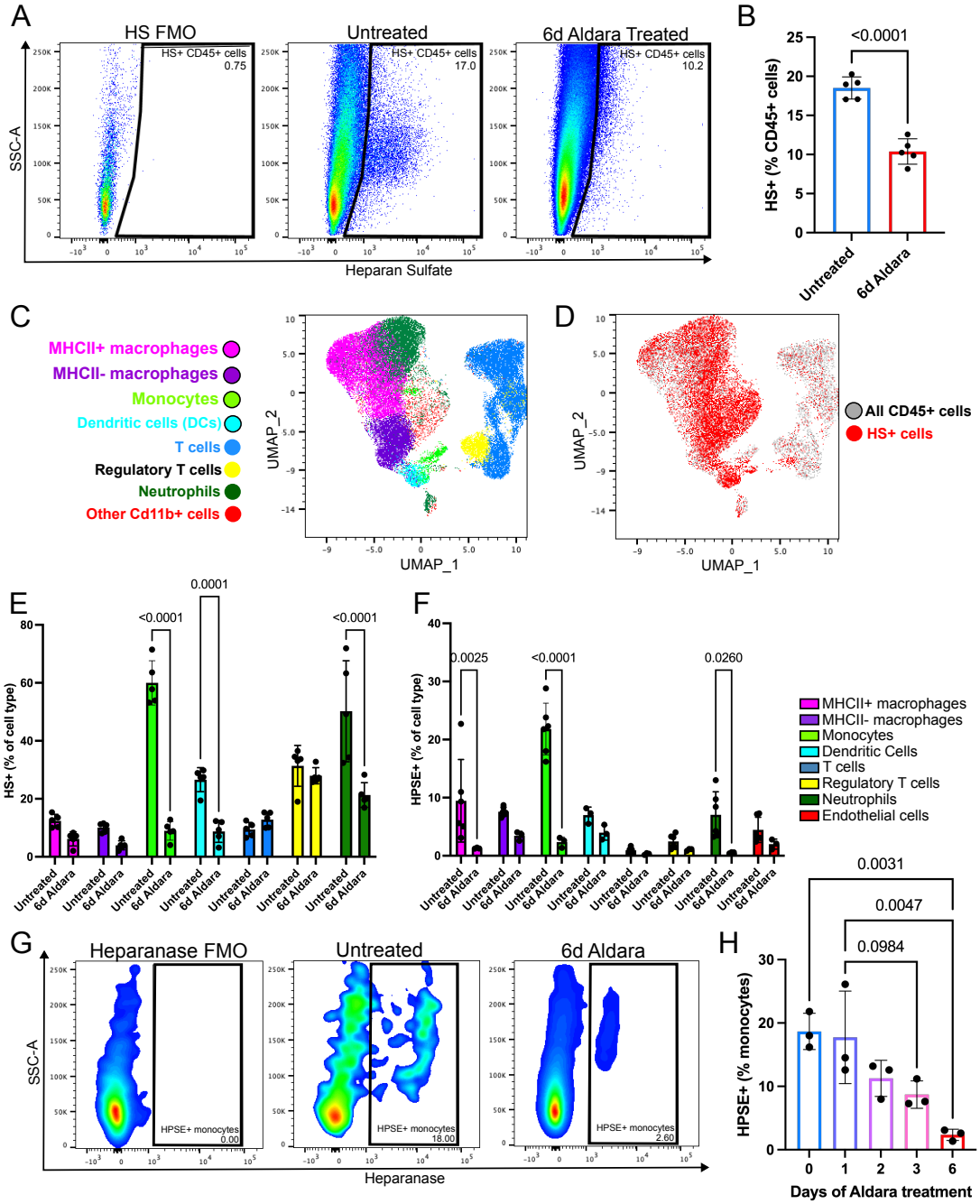

Figure 3. *Immune cells lose cell surface heparan sulfate in response to psoriasis-like skin inflammation.* Mice were treated topically with Aldara cream to the ear pinnae for 6 days. HS expression on immune cells was measured using flow cytometry (**A**) and the percentage of total CD45+ cells expressing HS was quantified in both untreated and Aldara treated skin (**B**). Naïve mouse skin was stained for flow cytometric analysis and major immune cell types were clustered using the UMAP algorithm (**C**). Cells positive for heparan sulfate (HS) were mapped onto the resulting clusters (**D**). The percentage of leukocyte subsets expressing HS with and without Aldara cream treatment is shown in **E**. Leukocytes were also stained intracellularly for the enzyme heparanase, and the proportions of cells positive for heparanase with and without Aldara cream

treatment are shown in **F**. Representative flow plots of monocyte heparanase staining are shown in **G** and the proportions of monocytes positive for heparanase with subsequent days of Aldara cream treatment is shown in **H**. Data show 2 independent experiments, except from **H** which is representative of 2 independent experiments. **A and G** show representative flow plots. Data in **B** were analysed by an unpaired t test, in **E and F** by 2-way ANOVA and **H** by 1-way ANOVA, both with Tukey's multiple comparisons test. Data with no p values shown are not significant ($p>0.05$). Error bars represent mean ± SD.

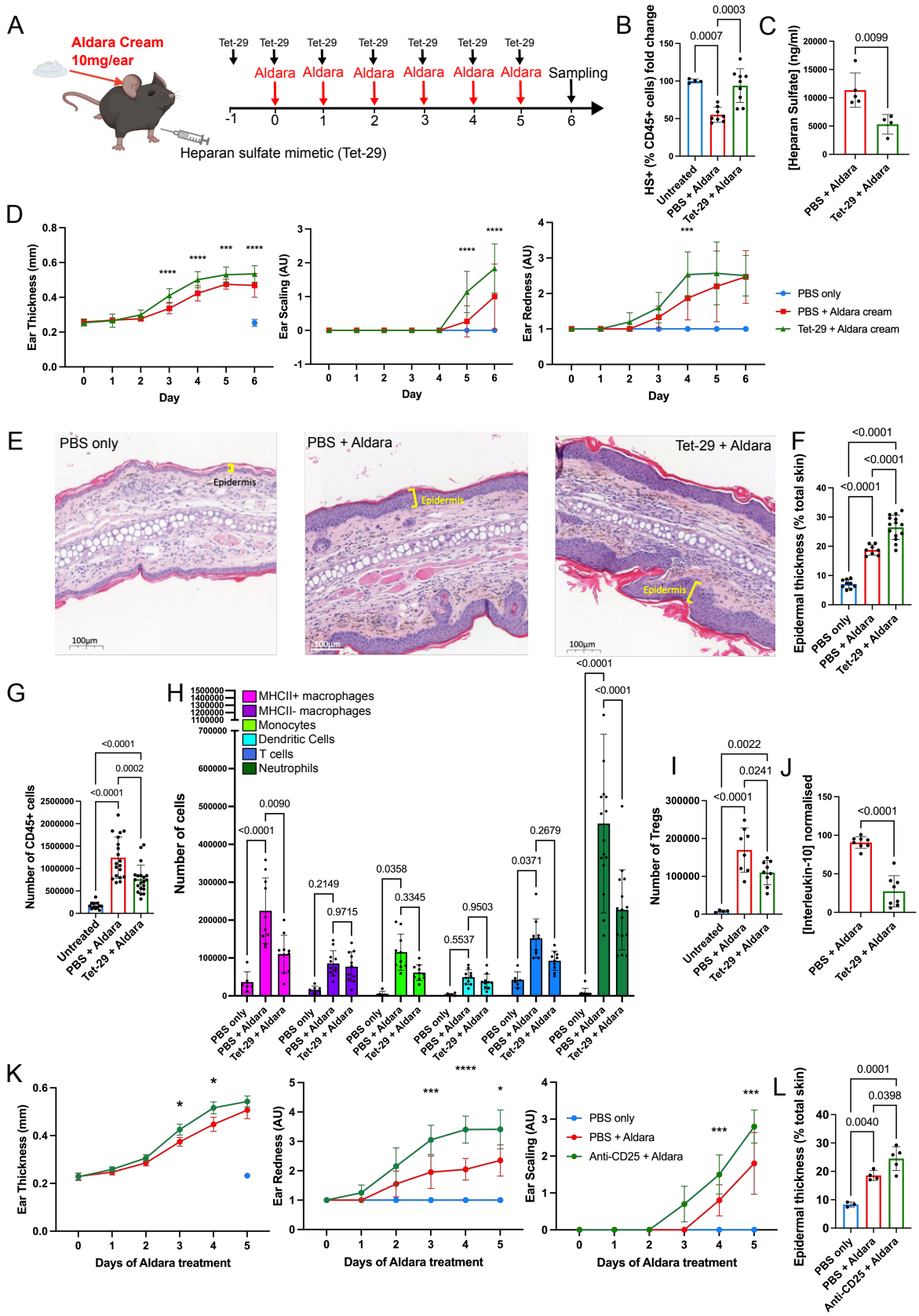
A
Aldara Cream
10mg/ear
Tet-29
Aldara
Sampling
Heparan sulfate mimetic (Tet-29)
B
HS+ (% CD45+ cells) fold change
Untreated
PBS + Aldara
Tet-29 + Aldara
C
[Heparan Sulfate] (ng/ml)
D
Ear Thickness (mm)
Ear Scaling (AU)
Ear Redness (AU)
Day
PBS only
PBS + Aldara cream
Tet-29 + Aldara cream
E
PBS only
PBS + Aldara
Tet-29 + Aldara
Epidermis
100µm
F
Epidermal thickness (% total skin)
G
Number of CD45+ cells
H
Number of cells
MHCII+ macrophages
MHCII- macrophages
Monocytes
Dendritic Cells
T cells
Neutrophils
I
Number of Tregs
J
[Interleukin-10] normalised
K
Ear Thickness (mm)
Ear Redness (AU)
Ear Scaling (AU)
Days of Aldara treatment
PBS only
PBS + Aldara
Anti-CD25 + Aldara
L
Epidermal thickness (% total skin)

677

678 **Figure 4.** *A heparan sulfate mimetic reduces heparan sulfate loss in leukocytes in response to skin*
679 *inflammation, inhibiting their accumulation in skin, yet enhances clinical signs of inflammation.*
680 Mice were treated topically with 10mg Aldara cream to the ear pinnae daily for 6 days (d0 to 5),
681 alongside intraperitoneal injection of the heparan sulfate mimetic, Tet-29, daily for 7 days (d -1 to
682 5) (**A**), or PBS was injected as a control. Total CD45+ cells were stained for HS and analysed by
683 flow cytometry (**B**). Levels of heparan sulfate in the blood were measured by ELISA (**C**). Clinical
684 signs of inflammation were monitored by measuring ear thickness using callipers and visually
685 scoring ear redness and ear scaling (**D**). Skin was sectioned and stained using haematoxylin and
686 eosin (H&E) (**E**) and epidermal thickness measured from images and calculated as a % of total ear
687 thickness (**F**). Total numbers of CD45+ cells were quantified (**G**) as well as numbers of
688 macrophages, monocytes, dendritic cells, T cells, neutrophils (**H**) and regulatory T cells (**I**) by
689 flow cytometry. Levels of interleukin-10 were measured in skin by ELISA (**J**). Mice were treated
690 with a Treg depleting antibody (anti-CD25) during the course of Aldara cream treatment; ear
691 thickness was measured using callipers and ears were visually scored for redness and scaling (**K**).
692 Aldara and anti-CD25 treated skin was also stained using H&E and epidermal thickness calculated
693 as a % of total ear thickness (**L**). Histology scale bars in **E** show 100 µm. **D, F, G and H** are pooled
694 data from 4 independent experiments. Data in **B, C, I, J, K and L** are pooled from 2 independent
695 experiments. Data in **D, H and K** were analysed using a two-way ANOVA with Tukey's multiple
696 comparisons test, except for redness and scaling measurements which are discontinuous variables
697 and so a Kruskal-Wallis with Dunn's multiple comparisons was used. **B, F, G, I and L** were
698 analysed by two-way ANOVA with Tukey's multiple comparisons test, and **C and J** by unpaired
699 t test. AU = arbitrary units. Error bars represent mean ± SD.

700

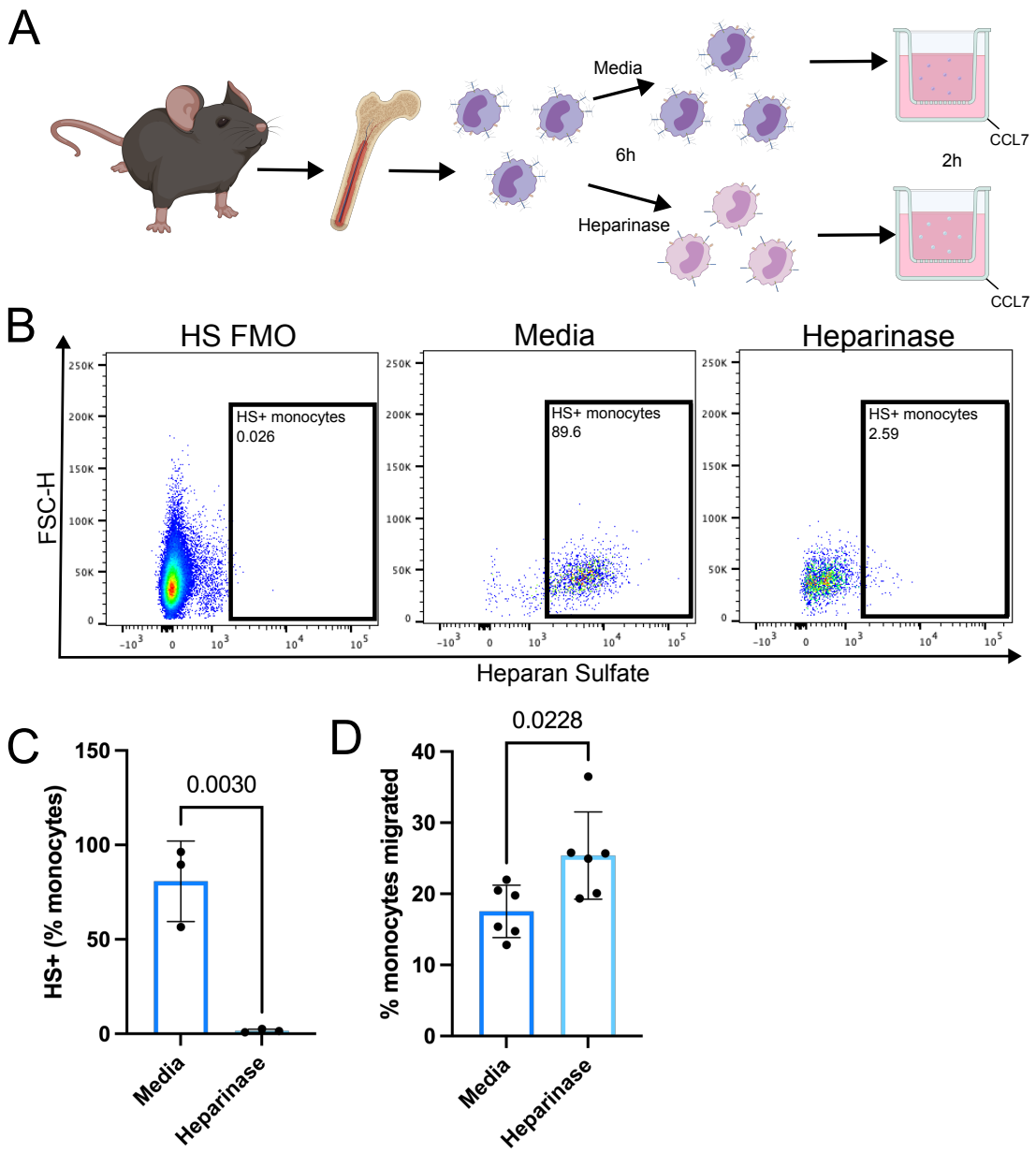

Figure 5. *Degradation of heparan sulfate on the surface of monocytes increases their ability to migrate in vitro*. Mouse bone marrow was cultured with or without heparinase I and III before being added to the top well of a transwell (**A**). Cells were allowed to migrate towards CCL7 for 2h and migrated cells were collected stained for heparan sulfate and analysed by flow cytometry (**B**) and the proportion of transmigrated monocytes expressing HS was calculated (**C**) along with the percentage of total monocytes that had migrated (**D**). Data are from 2 independent experiments each with 3 technical replicates. **B** shows representative flow plots. Data were analysed using an unpaired t test. Error bars represent mean ± SD.

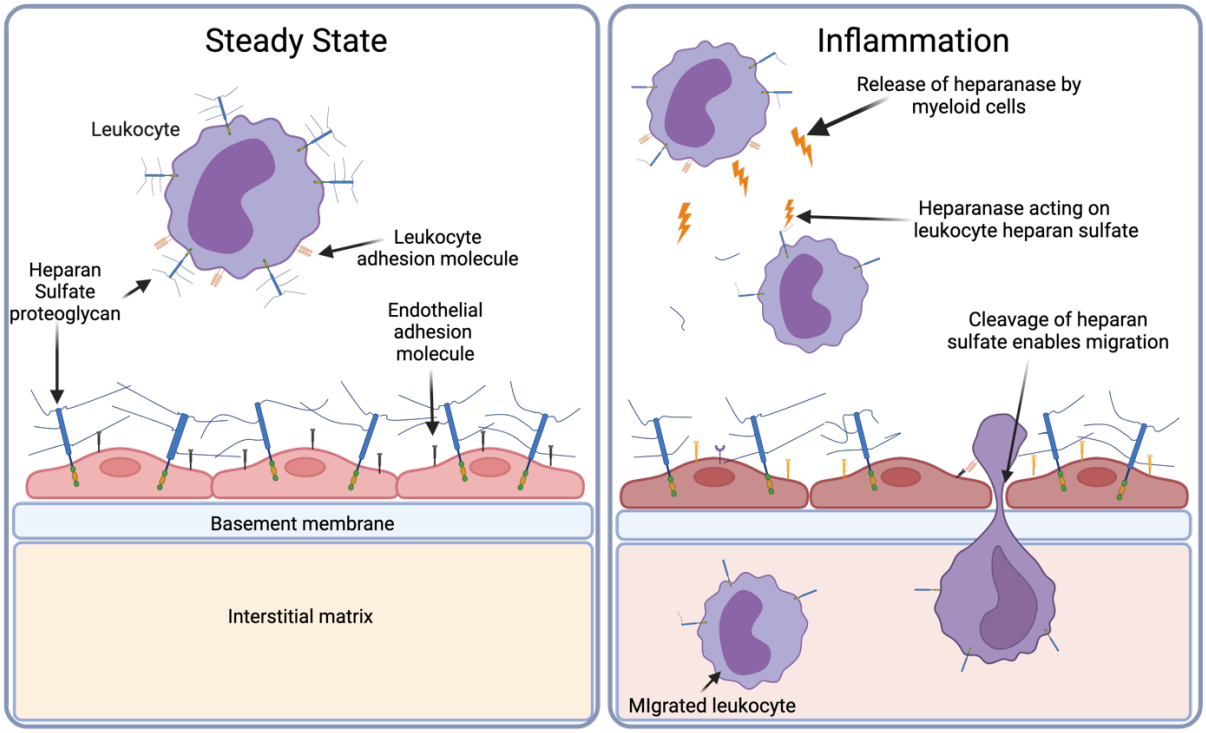

Figure 6. *Heparan sulfate shedding from the leukocyte glycocalyx enables their infiltration into the skin during psoriasis-like skin inflammation.* We propose that the leukocyte glycocalyx acts as a barrier to migration and is shed during inflammation to enable migration to inflammatory sites. Adapted from Sutherland et al. 2023.